Spectra and Photochemistry of Trifluoronitromethane Adsorbed on Alkali Halide Films

Mariaelena Galie, Janine M. Rusnock, Michael E. Yevich, and Christopher A. Baumann*

Department of Chemistry, The University of Scranton, Scranton, Pennsylvania 18510-4626

Received: June 18, 1997[⊗]

The infrared spectrum of trifluoronitromethane (CF_3NO_2) physically adsorbed on sublimated alkali halide (NaCl, NaBr, KCl, and KBr) films in submonolayer and multilayer coverages, and isolated in argon and nitrogen matrices, has been observed. The fundamental vibrations exhibit some surface-specific shifts, and there is indication that rotation about the CN bond is hindered upon adsorption. As in the gas phase, ultraviolet irradiation of the adsorbed species leads to the production of adsorbed carbonyl fluoride (CF_2O), but an adsorbed FNO photoproduct was not observed, presumably lost to a secondary photolysis. Quantum efficiencies for photolysis were determined for submonolayer and multilayer species and were found to be independent of temperature ($\Phi = 0.20 \pm 0.20$ adsorbed; 0.29 ± 0.20 multilayer), reduced from that of the matrix-isolated species. These quantum efficiencies were used to determine rate constants for surface-induced relaxation of the adsorbate as a function of surface composition and temperature. Desorption isotherms for both CF_3NO_2 and CF_2O were observed and fit to a first-order kinetic model of desorption, with activation energies of desorption of 14 ± 5 kJ mol^{-1} for CF_3NO_2 on the sodium salts, 16 ± 5 kJ mol^{-1} for CF_3NO_2 on the potassium salts, and 28 ± 6 kJ mol^{-1} for CF_3NO_2 desorbing from overlayers.

Introduction

The effect of adsorption on photochemical processes has been investigated over a wide range of substrates and adsorbates. Alkali halide surfaces have been among the most widely studied of the dielectric substrates, owing to their transparence over a large portion of the spectrum, their well-characterized structures, and their ability to physisorb molecules without undergoing chemical reaction. Much of the experimental[1,2] and theoretical[3−5] emphasis has been on molecules adsorbed onto LiF (001), although sublimated films of alkali halides have also been used.[6−10] Previous studies from this laboratory have demonstrated an alkali halide film's ability to quench the 600−700 nm photolysis of adsorbed trifluoronitrosomethane (CF_3NO).[10]

The trifluoronitromethane (CF_3NO_2) molecule has not received the same degree of attention as its nitroso analogue. The molecule's infrared spectrum has been observed and characterized,[11,12] although there have been differing estimates of the barrier to internal rotation, and hence, torsional frequency, arising from a coupling between the torsional mode and other low-frequency vibrations, presenting different apparent barriers to microwave and electron diffraction measurements.[13−17] The gas phase photochemical stability of CF_3NO_2 has also been studied. Absorption at 277 nm has been attributed to an n,π^* transition,[19] followed by rupture of the C−N bond. Further information has been accumulated through observation of its radical fragments: kinetics of the reaction between CF_3 and NO_2 have been studied in the gas phase,[19−21] as have those for the reaction between CF_3O and NO.[22−24]

In this paper, we report the results of our investigation into the photochemistry of CF_3NO_2 adsorbed onto sublimated films of NaCl, NaBr, KCl, and KBr. The molecule was also observed in solid nitrogen and argon matrices. The ($\lambda < 400$ nm) excitation of the adsorbed CF_3NO_2 leads to the production of CF_2O and FNO, but the nascent FNO appears to undergo subsequent photolysis. Shifts of the adsorbate vibrational bands from their gas phase values will be presented and used in the prediction of a possible mode of adsorption. Thermal desorption data for the adsorbate and its carbonyl fluoride product were fit to assumed first-order mechanisms, from which activation energies were obtained. A comparison of the matrix, adsorbed, and solid phase photochemistry will be useful in revealing the effects that the alkali halide surface has on the decomposition of this molecule.

Experimental Section

The experimental setup has been described in a previous paper.[10] The salt film was deposited on a window of the same alkali halide (NaBr was deposited on a NaCl window), maintained at 77 K via a Displex closed-cycle refrigerator. Infrared spectra were acquired on a Mattson Galaxy 5022 Fourier transform infrared spectrometer (DTGS detector). Background spectra of a clean film (after annealing, before adsorption) were acquired in the 4000−500 cm^{-1} region: all spectra were obtained as 32 coadded scans at 1 cm^{-1} resolution.

The CF_3NO_2 used in these experiments was (i) extracted from CF_3NO, (ii) observed as coadsorbate with the CF_3NO, or (iii) synthesized from CF_3NO using a method similar to that described by Fazekas and Takacs.[18] In the third method, a 200 Torr sample of CF_3NO (SCM Corporation Specialty Chemicals, Gainesville, FL) was added to a 500 mL flask containing 10 mL of freeze−thaw outgassed 30% H_2O_2 (Spectrum Chemical Mfg., Inc.). The sample was maintained above 340 K for several days and then the volatile fraction was distilled off using a dry ice−acetone bath (195 K). The collected volatiles were then further separated, using an ethanol slush bath (156 K) to remove the CF_3NO and other impurities more volatile than the CF_3NO_2. The gas was stored in an opaquely coated flask until its use.

Adsorbate pressure in the line was initially 50−70 Torr. Gas from the manifold was admitted into the cryostat via a stainless steel metering valve, through a length of thin nickel inlet tubing which enters the cryostat through the furnace. The tip of the inlet tube is directed at the window when the shroud is oriented for adsorption. Doses of the gas were admitted, usually 3−10

* Corresponding author. E-mail: CAB302@TIGER.UOFS.EDU. Fax: (717)941-7510.

[⊗] Abstract published in *Advance ACS Abstracts,* October 1, 1997.

S1089-5647(97)01995-0 CCC: $14.00

min at pressures below 2.2×10^{-6} Torr. The window was maintained at a temperature of 80 K during adsorption.

The shroud was then rotated into the position where the external windows were perpendicular to the optical beam, and the spectrum of the adsorbate was acquired. The temperature controller was then reset to 11 K, and a new spectrum was acquired at that temperature. The sample was then irradiated for a period of about 30 min. A spectrum was acquired following irradiation. Irradiations were performed using progressively shorter-wavelength sources, each followed by spectral acquisition. The source used for irradiation was a deuterium lamp (Beckman, Inc., 71701), filtered at $\lambda > 450$ nm, $\lambda > 420$ nm, or unfiltered. Some filtering was also achieved by irradiation through the NaCl external window (measured to have a transmittance of 30% at 200 nm, 68% at 250 nm) rather than the CaF_2 external window. This procedure was followed at progressively higher temperatures.

When the system has reached 85 K, the temperature was incrementally raised so that the different adsorbates (the originally adsorbed species and adsorbed photoproducts) were thermally desorbed. Unlike the usual methods of temperature-programmed desorption, the system was better suited to a stepped temperature profile: a temperature was selected, the desorption of a given species was followed by loss of infrared absorption in one or more of its infrared bands over the course of several minutes, and then a higher temperature selected. The temperature intervals chosen (5−10 K) were small enough to allow rapid (no more than several seconds) substrate equilibration. The desorption program was continued to 160 K, at which point all adsorbates had been desorbed. Due to the system geometry, the desorption of these species was unnoticed at the ionization gauge: presumably the abundance of cold surfaces along the pumpout pathway was sufficient to trap the desorbed species prior to the gauge tube. This also prevented the observance of isotherms of adsorption.

The matrix isolation experiments followed a similar procedure. The compound was synthesized as above, then mixed with the matrix gas (N_2, Ar: JWS Technologies, Inc., both prepurified grade) and stored in an opaquely glass flask. Dilutions of 1:18, 1:60, 1:560, and 1:3350 (CF_3NO_2:N_2) were prepared using standard manometric procedures. In the argon experiments, CF_3NO with a nominal 5−10% CF_3NO_2 impurity was mixed with argon in dilutions of 1:60, 1:700, and 1:2200 (CF_3NO:Ar). Both matrices had significant amounts of CF_3NO, as evidenced from their spectra. The matrices were deposited at a temperature of 20 K. In the matrix studies, the background spectra (also 32 scans at 1 cm^{-1} resolution) were acquired prior to the deposition of the matrix mixture.

Results

Vibrational Assignment of CF_3NO_2. The infrared spectra of CF_3NO_2 adsorbed on NaCl, NaBr, KCl, and KBr are shown in Figures 1−4, respectively. Combination bands were observed, all in the 900−1400 cm^{-1} region. These allowed the inferential assignment of low-frequency vibrations. No combinations involving the torsional mode were observed. Tables 1 and 2 contain the assigned values for the fundamentals and combinations and their shifts from the gas phase values. Overlayer spectra (an example is shown in Figure 5; assignments are found in Tables 1 and 2), which did not vary from substrate to substrate, were obtained as well. The largest vibrational shifts occur for the low-frequency structural vibrations, which, unfortunately, are also the vibrations measured with the smallest degree of accuracy, as they are only observed in combination in this study. In the gas phase, each of the rocking motions is doubly degenerate (due to free rotation about the C−N bond), and there is indication that this degeneracy is removed upon

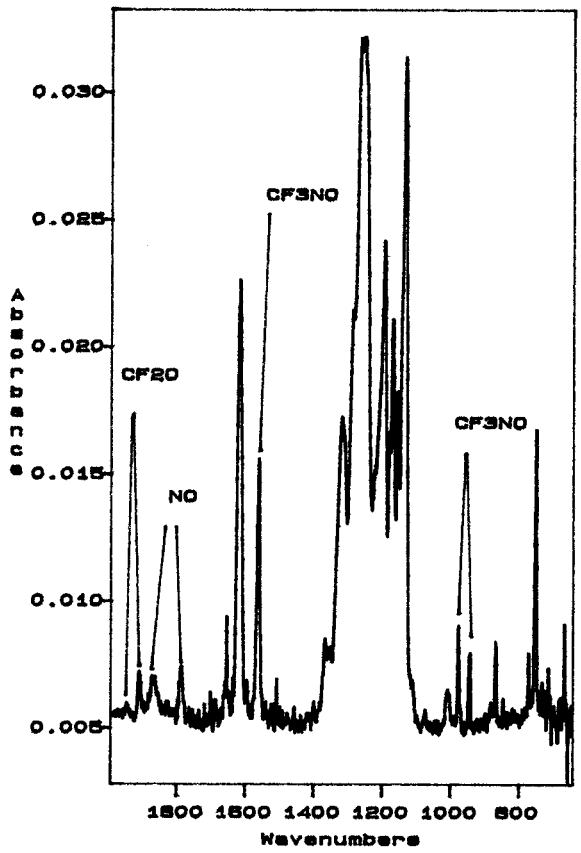

Figure 1. Infrared spectrum (1 cm^{-1} resolution, 32 coadded scans) of CF_3NO_2 adsorbed on a NaCl film at 80 K.

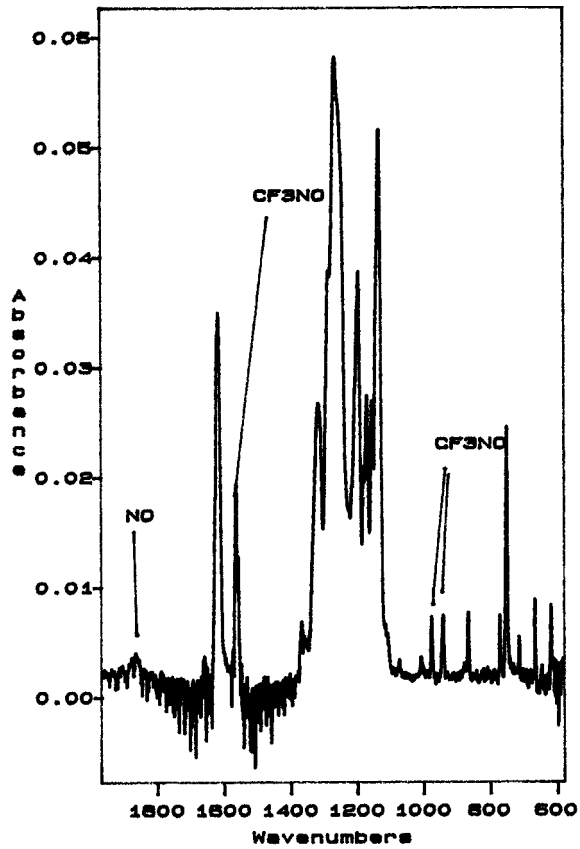

Figure 2. Infrared spectrum (1 cm^{-1} resolution, 32 coadded scans) of CF_3NO_2 adsorbed on a NaBr film.

TABLE 1: Observed Frequencies in the Infrared Spectrum of CF_3NO_2

frequencies (cm^{-1})							
	substrate				matrix		
overlayer	NaCl	NaBr	KCl	KBr	Ar	N_2	assignment
1605	1615	1618	1615	1617	1613	1620	ν_7 NO asymmetric stretch
1371	1365	1370	1366	1363	1364	1365	ν_3 CN stretch + ν_{13} CF_3 asymmetric deformation
						1324	ν_3 CN stretch + ν_{10} CF_3 rock
1309	1317	1316	1316	1319	1315	1314	ν_1 NO symmetric stretch
1283	1284	1284	1284	1286	1285	1284	ν_{12} CF asymmetric stretch
1262	1262	1263	1251	1250	1264	1269	ν_8 CF asymmetric stretch
					1257	1258	ν_3 CN stretch + ν_{11} NO_2 rock
1241						1251	ν_4 NO_2 symmetric deformation + ν_{13} CF_3 asymmetric deformation
1175	1192	1193	1193	1193	1210	1211	ν_4 NO_2 symmetric deformation + ν_{10} CF_3 rock
1158	1168	1168	1169	1169	1170	1173	ν_4 NO_2 symmetric deformation + ν_5 CF_3 symmetric deformation
1153	1153	1153	1153	1154	1155	1157	ν_2 CF symmetric stretch
1133	1131	1131	1132	1131	1141	1142	ν_4 NO_2 symmetric deformation + ν_{11} NO_2 rock
1104	1104	1108	1111	1106			$2\nu_9$ CF_3 asymmetric deformation
866	865	865	865	866	861	864	ν_3 CN stretch
750	749	749	749	749	749	750	ν_4 NO_2 symmetric deformation

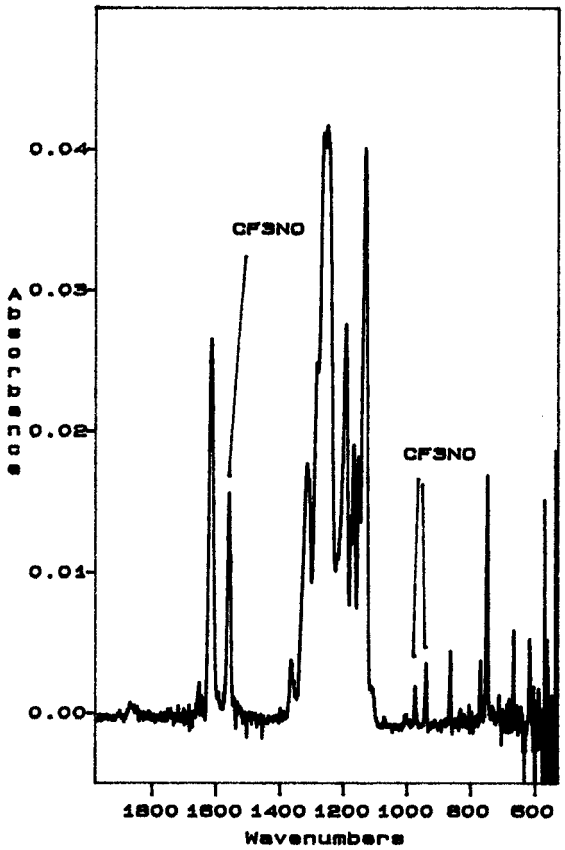

Figure 3. Infrared spectrum (1 cm^{-1} resolution, 32 coadded scans) of CF_3NO_2 adsorbed on a KCl film.

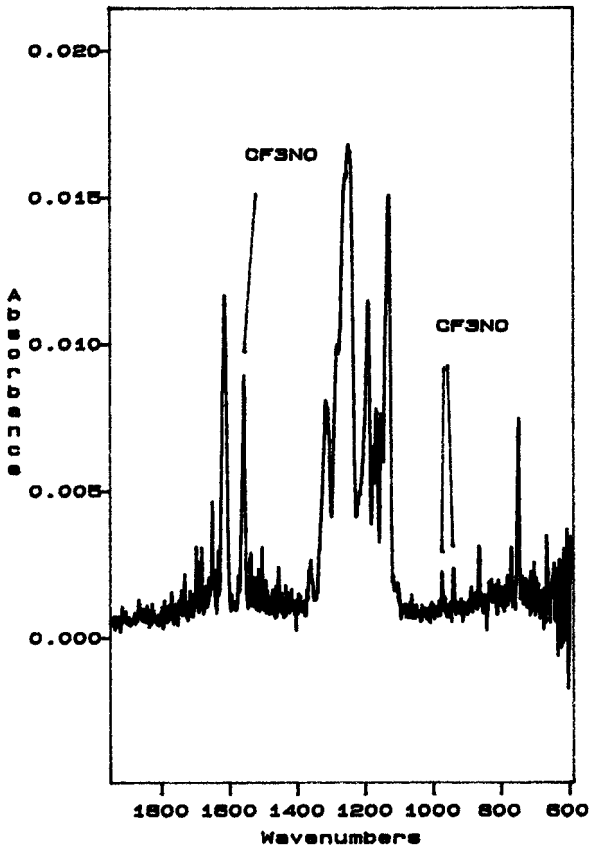

Figure 4. Infrared spectrum (1 cm^{-1} resolution, 32 coadded scans) of CF_3NO_2 adsorbed on a KBr film.

adsorption. The symmetric NO stretch is shifted ($\Delta\nu = 6-9$ cm^{-1}) on the films but is unshifted in the condensed phase. Conversely, the asymmetric NO stretch is only slightly shifted by the films (from -2 to -5 cm^{-1}) but is dramatically shifted in the condensed phase (-15 cm^{-1}). The C−N stretch is shifted (5−6 cm^{-1}) by adsorption with little variation from substrate to substrate. The C−F stretches vary from slightly shifted (the symmetric stretch is shifted by 2−3 cm^{-1}) to strongly shifted (ν_8 is shifted from -8 to -21 cm^{-1}). The magnitude and substrate dependence (the potassium halides exhibit shifts more than a factor of 2 larger than those of the sodium halide films) of the ν_8 shift indicates that there may be significant fluorine−cation interaction.

In the inert gas matrices, the fundamental vibrations are observed with only slight matrix-induced shifts: these are most pronounced in the more concentrated matrices, as are site-induced splittings. The infrared spectrum of CF_3NO_2 in a nitrogen matrix may be seen in Figure 6 and that in the argon matrix in Figure 7.

Photochemistry of CF_3NO_2. Ultraviolet irradiation of the adsorbed CF_3NO_2 produced features attributable to adsorbed CF_2O, for which a vibrational assignment is summarized in Table 3. The photolysis seemed to follow the gas phase results[18] except for the lack of observable FNO. Irradiation at temperatures from 12 to 90 K on a variety of alkali halides was attempted in order to determine if any conditions would produce features attributable to adsorbed FNO, but without success. Figure 8 (this difference spectrum was smoothed using a Savitsky−Golay cubic 5-point algorithm to reduce the effect of inadequately subtracted atmospheric water vapor) shows the

TABLE 2: Vibrational Assignment of Adsorbed and Matrix-Isolated CF_3NO_2

		frequencies and shifts (cm^{-1})													
			substrate							matrix					
mode	description	gas[a]	NaCl	$\Delta\nu$	NaBr	$\Delta\nu$	KCl	$\Delta\nu$	KBr	$\Delta\nu$	Ar	$\Delta\nu$	N_2	$\Delta\nu$	overlayer	$\Delta\nu$
ν_1	NO symmetric stretch	1310	1317	7	1316	6	1316	6	1319	9	1315	5	1314	4	1310	0
ν_2	CF symmetric stretch	1151	1153	2	1153	2	1153	2	1154	3	1155	4	1157	6	1153	2
ν_3	CN stretch	860	865	5	865	5	865	5	866	6	861	1	864	4	866	6
ν_4	NO_2 symmetric deformation	750	749	−1	749	−1	749	−1	749	−1	749	−1	750	0	750	0
ν_5	CF_3 symmetric deformation	430	419	−11	419	−11	420	−10	420	−10			423	−7		
ν_7	NO asymmetric stretch	1620	1615	−5	1618	−2	1615	−5	1617	−3	1613	7	1620	0	1605	−15
ν_8	CF asymmetric stretch	1271	1262	−9	1263	−8	1251	−20	1250	−21	1264	−7	1269	−2	1262	−9
ν_9	CF_3 asymmetric deformation	527	552	25	554	27	556	29	553	26					552	25
ν_{10}	CF_3 rock	441	443	2	444	3	444	3	444	3	461	20	460	19		
ν_{11}	NO_2 rock	400	382	−18	382	−18	383	−17	382	−18	396	−4	394	−6	383	−17
ν_{12}	CF asymmetric stretch	1288	1284	−4	1284	−4	1284	−4	1286	−2	1285	−3	1284	−4	1283	−5
ν_{13}	CF_3 asymmetric deformation	527	500	−27	505	−22	501	−26	497	−30	503	−24	501	−26	498	−29
ν_{14}	CF_3 rock	441											451	10		
ν_{15}	NO_2 rock	400									392	−8	392	−8	408	8

[a] Reference 12.

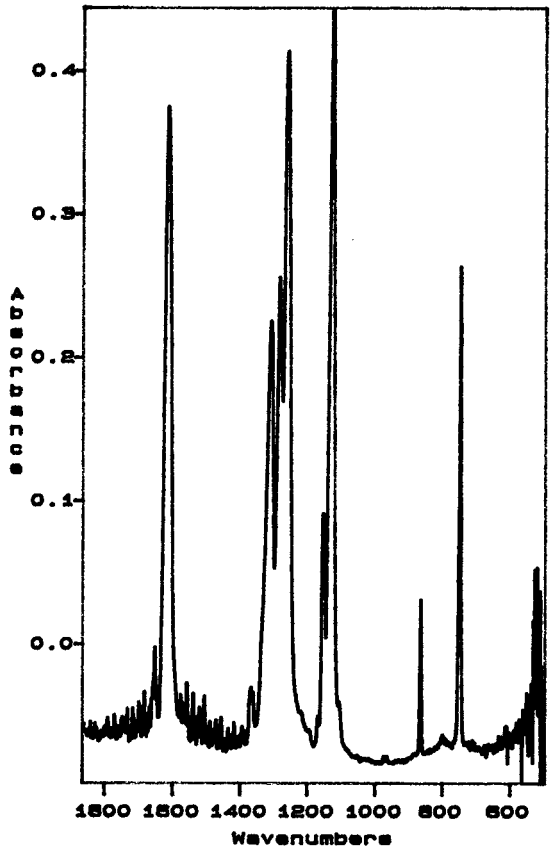

Figure 5. Infrared spectrum (1 cm^{-1} resolution, 32 coadded scans) of CF_3NO_2 in overlayer coverage.

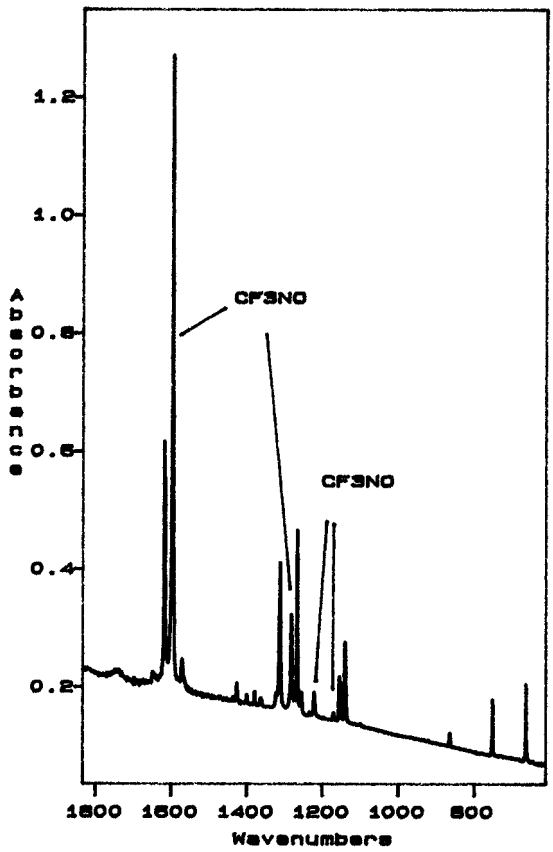

Figure 6. Infrared spectrum (1 cm^{-1} resolution, 32 coadded scans) of CF_3NO_2 in a nitrogen matrix (1:3350).

results of the photolysis on KCl; the irradiations on the other films give similar results. The absence of FNO can be explained by one or a combination of events: (a) the subsequent reaction of the nascent FNO with CF_3NO_2, other adsorbed species, or the surface; (b) the production of an FNO molecule that is free of the surface (the molecule is produced with an internal energy exceeding the binding energy to the surface or is never in contact with the surface during its formation); or (c) the infrared bands of the adsorbed FNO shifting to the extent that they lie under those for the other adsorbed species (the 1844 cm^{-1} FNO band under the 1907 cm^{-1} CF_2O band; the 766 cm^{-1} FNO band under the 751 cm^{-1} band of CF_3NO_2 or the 774 cm^{-1} band of CF_2O). Irradiation at the wavelengths over which the parent compound is photolyzed should also photolyze the FNO (to F and NO).[25] Any fluorine atoms produced by this secondary photolysis would certainly react with the surface, even at the low temperatures of these experiments. One such reaction would be the halogen exchange:

$$F + NaCl \rightarrow NaF + Cl \qquad \Delta H = -116 \text{ kJ mol}^{-1} \text{ (ref 26)} \tag{1}$$

but reactions involving electron excess surface defects (such as F or M centers) should also occur, given the prevalence of defects in the sublimated film.[27] The attachment of fluorine atoms to such surface defects would have very little impact on the observed infrared spectrum. Some evidence of dimeric NO[28] is observed when photolysis is carried out for longer periods of time (6+ h). A peak at ∼1184 cm^{-1} appeared in all photolyses on the alkali halide films.

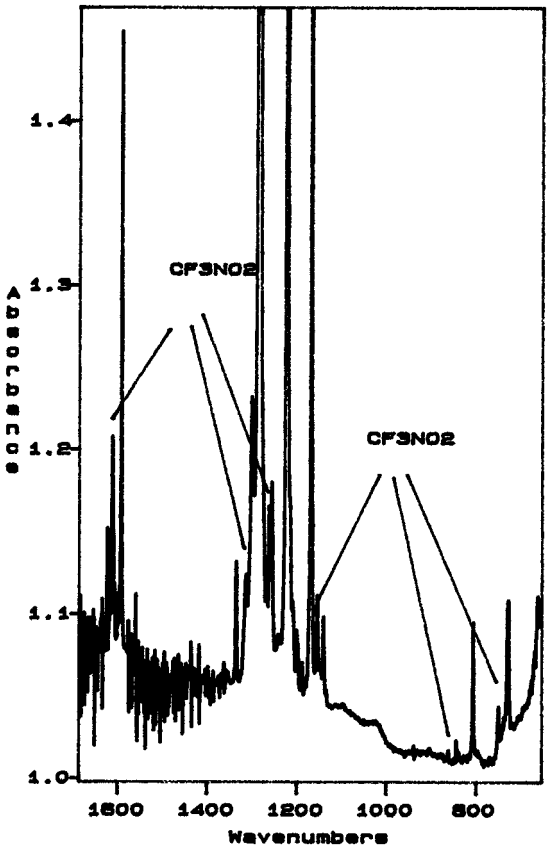

Figure 7. Infrared spectrum (1 cm^{-1} resolution, 32 coadded scans) of CF_3NO in an argon matrix (1:2200) with a CF_3NO_2 impurity (~5−10%).

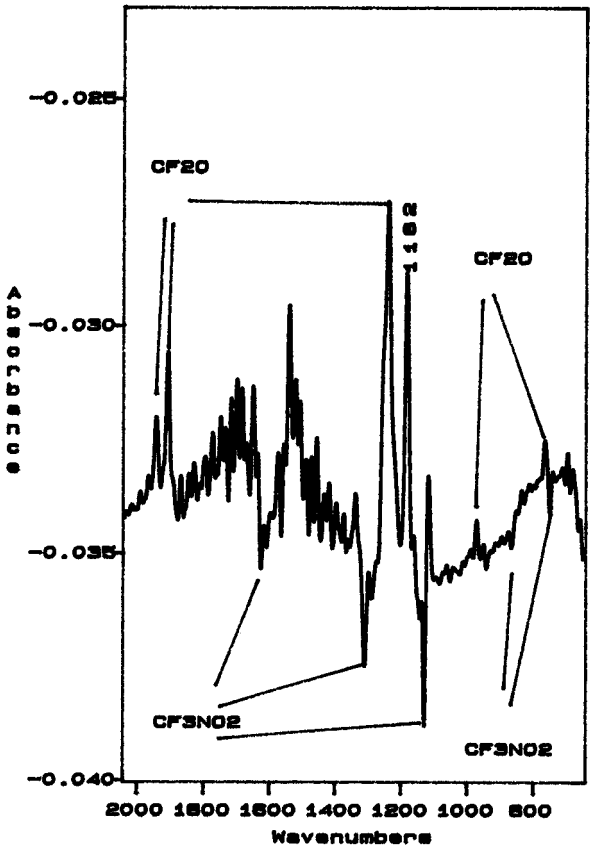

Figure 8. Infrared difference spectrum (1 cm^{-1} resolution, 32 coadded scans) of CF_3NO_2 adsorbed on a KCl film. The spectrum is the result of subtracting the preirradiation spectrum from the postirradiation spectrum. Positive peaks correspond to photolytic products, negative peaks correspond to species lost as a result of irradiation. This spectrum was smoothed to reduce the features due to inadequate subtraction of background water vapor.

TABLE 3: Observed Frequencies in the Infrared Spectrum of CF_3NO_2 Photoproducts

frequencies (cm^{-1})						
substrate				matrix		
NaCl	NaBr	KCl	KBr	Ar	N_2	assignment
					3369	
					2235	N_2O ν_3 asymmetric stretch
1935	1936	1938	1939	1935	1939	CF_2O ν_2 CO stretch
1906	1907	1908	1907	1909	1911	CF_2O $2\nu_1$ CF stretch
	1860			1884	1899	NO
				1872		*cis*-$(NO)_2$
					1860	CF_3OONO_2 NO stretch
				1826		
	1750	1746	1747		1766	*cis*-$(NO)_2$
					1314	
					1289	N_2O ν_1 symmetric stretch/ CF_3OONO_2 NO_2 stretch
1243	1247	1238	1239	1247	1246	CF_2O ν_4 CF stretch
					1236	CF_3OONO_2 CF stretch
					1217	
				1210	1211	
					1188	CF_3OONO_2 CF stretch
1186	1183	1184	1184			
					1166	
		1117	1117			
			1032		1042	
971	969	969	972	964	965	CF_2O ν_1 CF stretch
					957	CF_3OONO_2 CO stretch
					789	CF_3OONO_2 NO_2 scissor
761	765	760	764	770	766	CF_2O ν_6 deformation
					741	
				718	712	
	694	694	695	694		
					622	CF_2O ν_3 CF_2 bend

FNO is not observed in the matrix experiments. Peaks attributable to CF_2O, N_2O, and NO are observed in the nitrogen matrices after photolysis. A set of peaks appears at 1766, 1236, 1188, 957, and 789 cm^{-1}. These are presumably due to CF_3OONO_2, which has been observed by Horst and DesMarteau[29] in the liquid phase and Chen *et al.*[22] in the gas phase. These peaks did not appear in the argon matrix experiments. The additional oxygen for the peroxy compound may have come from oxygen impurities in the nitrogen, from the secondary photolysis of the FNO, or perhaps from a second decomposition pathway of the parent compound, in which an NO bond, rather than the CN bond, is cleaved. This has been observed in CH_3NO_2[30] but has not been reported for CF_3NO_2. The nitrogen matrices show many more peaks upon photolysis, undoubtedly due to the ability of the matrix to react with the fluorine and/or oxygen atoms produced in the secondary photolysis of the FNO. A number of the unassigned peaks are possible $N_xH_yF_z$ species, with the hydrogens coming from water or other matrix impurities. The peaks observed at 3369 and 1042 cm^{-1} following photolysis in the most dilute nitrogen matrix may be attributed to one such species: these peaks are in the region expected for NH and NF stretching modes, respectively, but cannot be assigned to any of the NH_yF_z ($y = 1, 2$; $z = 2, 1$) found in previous inert gas matrix experiments[31−33] or to the combined spectra of NF and NH.[32,34] The frequency of this NH stretch lies near where one would predict that for the previously unobserved NH_2F would occur, given the higher observed frequency in NH_3,[35] the lower one in NHF_2,[32] and the similar frequency found in NH_2Cl.[36] However, it would be presumptuous to state that the species is NH_2F in the absence of more definitive data. In the argon matrix, reaction between the matrix and the fluorine atoms will not occur, and the resulting infrared

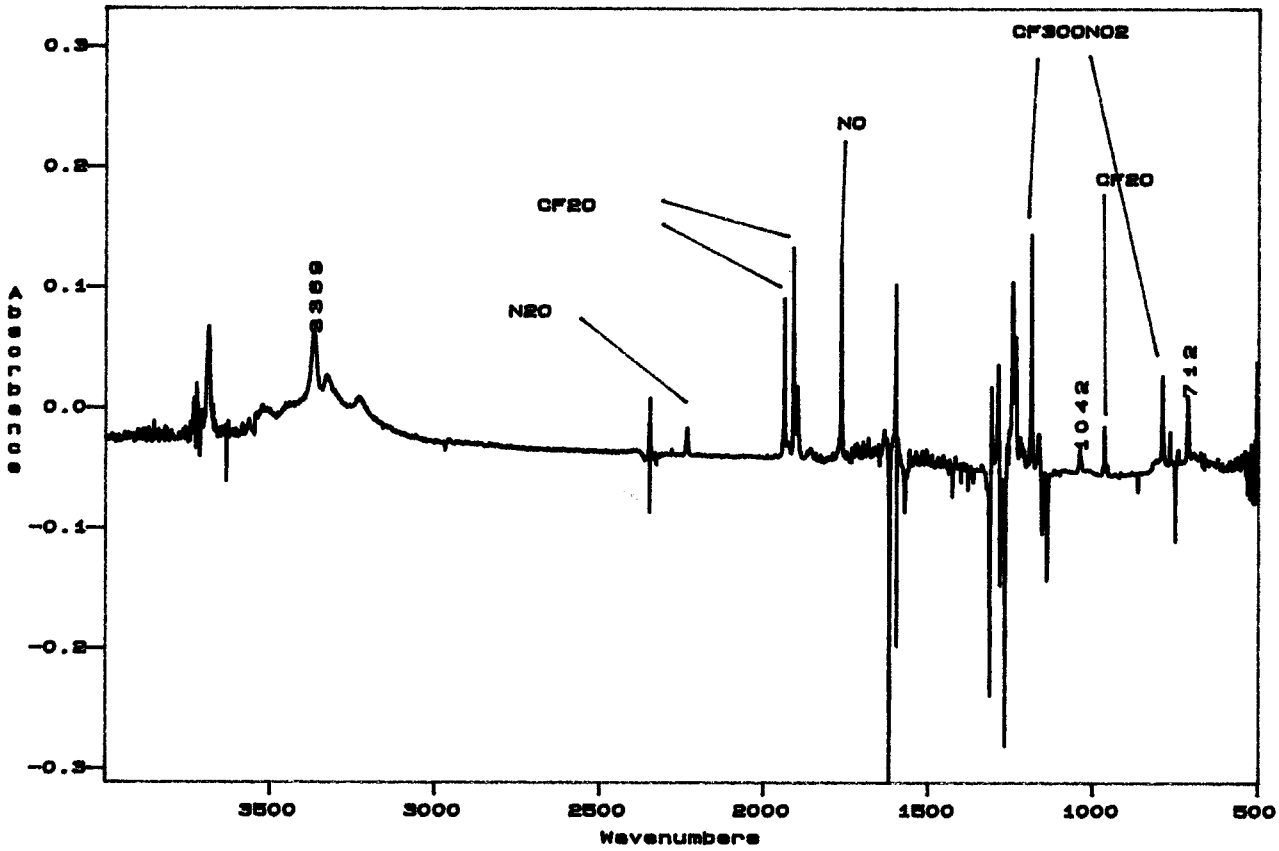

Figure 9. Infrared difference spectrum (1 cm^{-1} resolution, 32 coadded scans) of CF_3NO_2 in a nitrogen matrix (1:3350). The spectrum is the result of subtracting the preirradiation spectrum from the postirradiation spectrum. Positive peaks correspond to photolytic products, negative peaks correspond to species lost as a result of irradiation.

spectra show far fewer peaks. Difference spectra, in which the preirradiation spectrum was subtracted from the postirradiation spectrum, are shown for the matrix-isolated species in Figures 9 and 10. Irradiation of the nitrogen matrix through the calcium fluoride external window did not appear to change the relative distribution of photoproducts, but did result in a 10-fold increase in the overall photolysis, which may be attributed to the enhanced UV transmittance of the CaF_2 window relative to the NaCl external window.

The quantum efficiency was calculated from the loss of CF_3NO_2 infrared absorption and gain of CF_2O absorption:[37]

$$\Phi = \frac{\Delta N_{CF_3NO_2}}{N_{\text{absorbing}}} = \frac{\Delta A_{ir} a}{t\epsilon_{ir} I_0 (1 - 10^{-A_{uv}})} \qquad (2)$$

where A_{ir} is the infrared absorbance, a the area (in cm^2) of the adsorption window in the infrared beam, t the duration of the irradiation period (in seconds), ϵ_{ir} the extinction coefficient for the particular infrared band (in cm^2 mol^{-1}), I_0 the intensity of the incident radiation (einstein s^{-1}) in the region of photolysis, and A_{uv} the absorbance of the sample at the wavelength of irradiation. Attempts to determine the absorbance in the visible simultaneously with the infrared absorbance proved fruitless, owing mostly to the scattering of the incident light by the film. Therefore, the gas phase extinction coefficients, in combination with the infrared absorbances, were used to calculate UV absorbances (IR and UV cross sections were obtained from refs 12 and 18, respectively). Thus

$$\Phi = \frac{\Delta A_{ir} a}{t\epsilon_{ir} I_0 (1 - 10^{-A_{ir}(\epsilon_{uv}/\epsilon_{ir})})} \qquad (3)$$

becomes the equation used in these calculations. The extinction coefficients for the adsorbed molecules were assumed to be identical to their gas phase values, both in the ultraviolet and infrared, and are listed in Table 4. The ultraviolet extinction coefficients from ref 18 were averaged over the wavelengths transmitted by the external windows. The CF_3NO_2 bands followed were ν_7 (~1615 cm^{-1}), ν_3 (~865 cm^{-1}), and ν_4 (~749 cm^{-1}). Photolysis was also followed by observing the production of the CF_2O, using the bands in the Fermi doublet in the 1940−1900 cm^{-1} region. The extinction coefficients for the CF_2O were extracted from spectra in ref 37. The quantum efficiencies obtained from the loss of the parent compound were in agreement with those obtained from the gain of photoproduct, except at substrate temperatures of 80 K and above.

The intensity of the incident radiation was determined by setting the matrix isolation quantum efficiency to unity and then solving for the intensity in the photochemically useful part of the spectrum. The intensity (averaged over several experiments with both matrix gases, using the same vibrations of parent and product species as described above) was then used in the determination of the adsorbed phase efficiency. This assumes that the absorption in the ultraviolet is not shifted significantly by adsorption. The results of the irradiation experiments are summarized in Table 5.

An identical procedure was followed for the multilayer species. Figure 11 contains a difference spectrum for photolysis of CF_3NO_2 in multilayer coverage; the results of the multilayer photolyses are also contained in Table 5.

Thermal Desorption Kinetics. The thermal desorption of CF_3NO_2 was followed at temperatures from 90 to 110 K. As with the photochemistry studies, absorbances of the ν_7, ν_3, and ν_4 peaks were measured as a function of time and temperature.

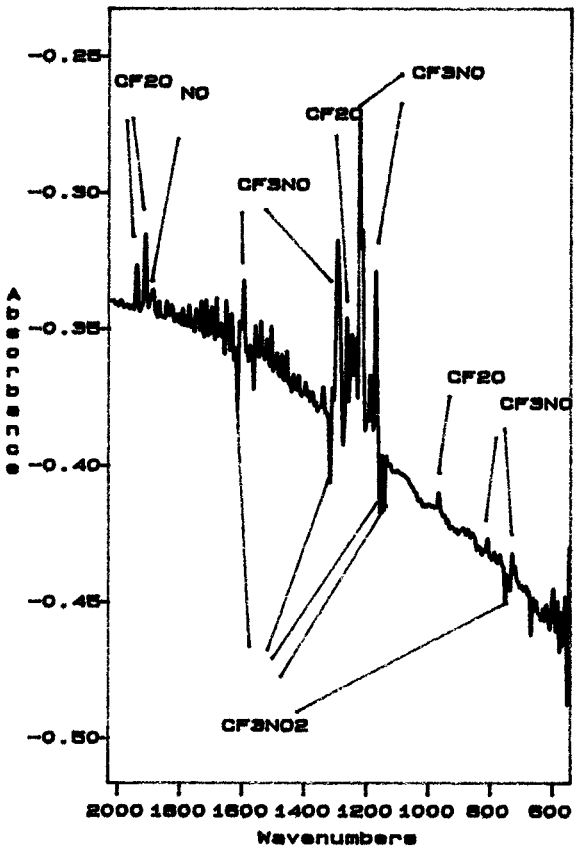

Figure 10. Difference spectrum of $CF_3NO + CF_3NO_2$ in an argon matrix (1:2200). The spectrum is the result of subtracting the preirradiation spectrum from the postirradiation spectrum. Positive peaks correspond to photolytic products, negative peaks correspond to species lost as a result of irradiation. This spectrum was smoothed to reduce the features due to inadequate subtraction of background water vapor.

TABLE 4: Infrared and Visible Extinction Coefficients for CF_3NO_2 and CF_2O

species	wavenumber (cm^{-1})	wavelength (nm)	ϵ_{ir} (cm^2 mol^{-1})[a,b]	ϵ_{uv} (cm^2 mol^{-1})[c]
CF_3NO_2	1610		17 3000	
	865		12 200	
	750		43 200	
		200−300		1.2×10^6
CF_2O	1940		20 600	
	1907		32 100	

[a] CF_3NO_2 values obtained from spectrum in ref 12. [b] CF_2O values obtained from spectrum in ref 37. [c] Obtained from spectrum in ref 18.

These particular peaks were chosen due to their relatively high intensities and their location away from interfering spectral regions. The desorptions appeared to follow first-order kinetics, with least-squares correlation coefficient (R^2) values in excess of 0.87 for all of the first-order plots. Similarly, the photoproduct CF_2O Fermi doublet peaks were followed, also showing clear first-order desorption kinetics. A desorption plot for CF_3NO_2 on KCl in which the natural logarithm of the average normalized peak height is plotted vs time may be found in Figure 12. A similar plot for CF_2O on KCl is shown in Figure 13. The plots for the other substrates show similar features.

At each temperature, a first-order rate constant (k) was determined from the slope of the desorption plot. The rate constants were then used to determine the activation energy of desorption from the slope of an Arrhenius plot (ln k vs $1/T$). Figures 14 and 15 show the Arrhenius plots for CF_3NO_2 and CF_2O, respectively, on KCl. The activation energies and preexponential terms obtained for the two species may be found in Table 6. The reader is reminded that the preexponential terms are not strictly single vibrational frequencies; rather, they incorporate, among other effects, the degree to which the molecule samples a number of surface sites during its desorption. As a result, the preexponential terms will vary substantially from one film to the next, depending on the degree of film corrugation.

TABLE 5: Quantum Efficiencies (Based on CF_3NO_2 Loss and CF_2O Gain) for Photolysis of Adsorbed CF_3NO_2

substrate	temp (K)	Φ (±0.20)
NaBr	10	0.08
	70	0.20
KCl	80	0.09
	80	0.31
	80	0.12
KBr	10.5	0.31
	80	0.20
	80	0.24
	95	0.22
overlayer	11.2	0.29
	11.6	0.28
	50	0.35
	80	0.32
	80	0.12
	50	0.40

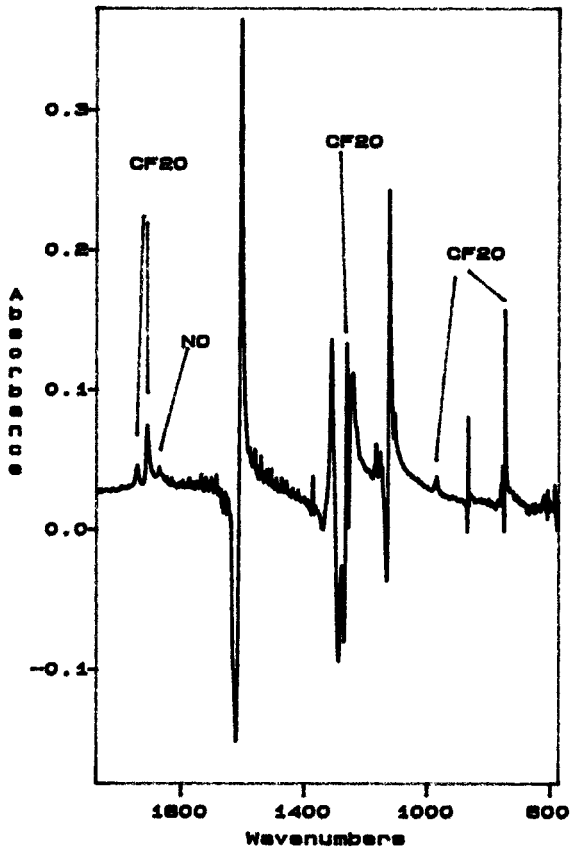

Figure 11. Infrared difference spectrum (1 cm^{-1} resolution, 32 coadded scans) of CF_3NO_2 in multilayer coverage. The spectrum is the result of subtracting the preirradiation spectrum from the postirradiation spectrum. Positive peaks correspond to photolytic products, negative peaks correspond to species lost as a result of irradiation.

Discussion

Vibrational Spectrum of Adsorbed CF_3NO_2. The removal of the degeneracies of the CF_3 asymmetric deformation motions

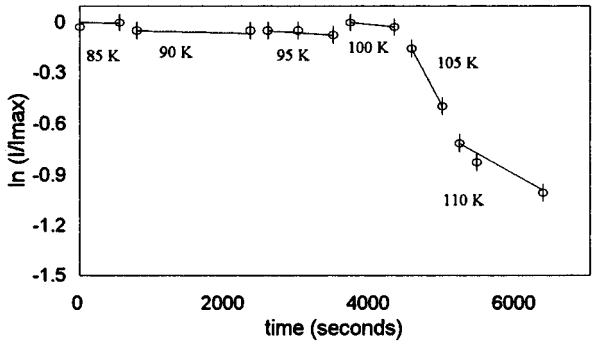

Figure 12. Thermal desorption of CF_3NO_2 from a KCl film. The natural logarithm of the reduced infrared absorbance ($A = A_t/A_{max}$) is plotted as a function of time. The lines represent the derived first-order rate constants to desorption at the particular temperature.

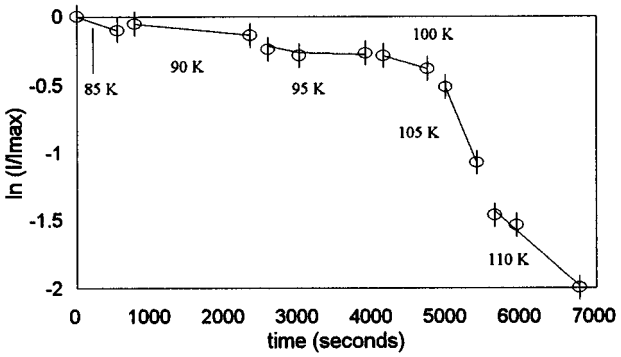

Figure 13. Thermal desorption of CF_2O from a KCl film. The natural logarithm of the reduced infrared absorbance ($A = A_t/A_{max}$) is plotted as a function of time. The lines represent the derived first-order rate constants to desorption at the particular temperature.

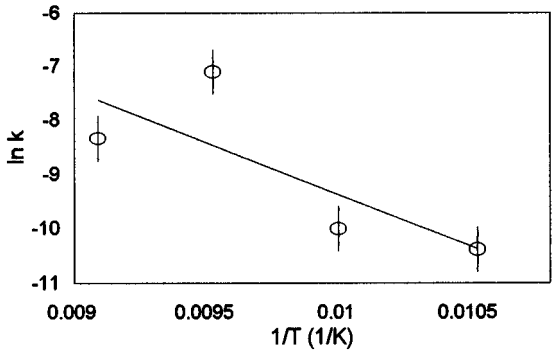

Figure 14. Arrhenius plot for the thermal desorption of CF_3NO_2 from a KCl film. The line is a least-squares linear regression fit to the observed first-order rate constants.

upon adsorption is expected, given that the degeneracies in the gas phase are the result of free rotation (see refs 13−17) about the CN bond. The molecule is apparently adsorbed in a configuration that hinders the motion about the CN bond, and this hindrance is large enough that no vibrations show any temperature dependence in width, frequency, or relative intensity from 10 to 110 K. This conclusion would more definitive if both components of the CF_3 and NO_2 rocking modes were also observed. The deformation mode of the nitro group exhibits little shift upon adsorption, and no significant ion dependence is observed. The CN stretch likewise shows no trend from surface to surface, nor do two of the three C−F stretches. The vibrational shifts described above, and the dependence of the shift of ν_8 on the surface cation is consistent with an adsorption geometry similar to that determined for CF_3NO on these surfaces,[10] where the C−N bond is parallel to the surface and

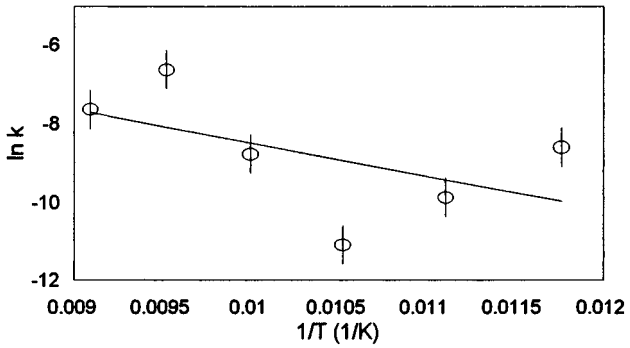

Figure 15. Arrhenius plot for the thermal desorption of CF_2O from a KCl film. The line is a least-squares linear regression fit to the observed first-order rate constants.

TABLE 6: Desorption Parameters for CF_3NO_2 and CF_2O

molecule	surface	E_a (kJ mol^{-1})	A (s^{-1})
CF_3NO_2	NaCl	14 ± 5	3×10^3
	NaBr	14 ± 5	8×10^3
	KCl	16 ± 5	5×10^3
	KBr	16 ± 5	2×10^4
	overlayer	28 ± 6	9×10^{11}
CF_2O	NaCl	4 ± 3	0.01
	NaBr	13 ± 4	7×10^3
	KCl	6 ± 4	9.4
	KBr	10 ± 4	37

pointed in the [110] direction and the trifluoromethyl group pointed toward the cation.

The spectra of the submonolayer and overlayer species may be clearly distinguished by the difference in the stretching frequencies associated with the nitro group.

Desorption of CF_3NO_2 and CF_2O. The desorption of both species seems to be consistent with first-order kinetics. Each follows an Arrhenius temperature dependence, particularly at higher temperatures. The relatively small differences between the frequencies of low and multilayer coverage CF_3NO_2 species indicate that the molecules may be forming islands on the surface, rather than adsorbing in submonolayer fashion. This means that the desorptions observed will represent those from isolated surface sites and from atop other adsorbed molecules. Desorptions from overlayer coverages were also fit to first-order desorption kinetics, but with measured desorption activation energies approaching 25 kJ mol^{-1} (the latent heat of vaporization near the boiling point of 242 K was measured by Banus[38] and also Jander and Haszeldine[39] to be 22−25 kJ mol^{-1}) and preexponential terms exceeding 5×10^8 s^{-1}. If this is an accurate depiction of the adsorbate−adsorbate interaction energy, then CF_3NO_2/MX represents a system for which the molecule−molecule attraction exceeds the molecule−surface attraction, making it difficult to distinguish those effects due to molecule−surface interactions from those involving bimolecular events, even in low coverage.

Photochemistry of CF_3NO_2. The measurement of quantum efficiency using the loss of parent compound alone would result in higher apparent values at the higher temperatures, as some of the parent is lost through purely thermal desorption. Basing the measurement strictly on photoproduct gain would result in lower apparent values at higher temperatures, as the photoproduct CF_2O desorbs at an even lower temperature than the parent. There does not seem to be any temperature dependence to the measured efficiencies on these surfaces, in submonolayer or overlayer coverages, from 10 to 95 K. Above 80 K, thermal desorption rates are high enough to limit our ability to accurately measure the quantum efficiency. There seems to be no tem-

perature dependence to the quantum efficiency in the matrix, although the temperature range available is much smaller. The values for the quantum efficiencies were determined with the assumption that the inert gas matrix quantum efficiency was unity, so any diminution of the matrix value will also result in a diminished apparent surface value.

The reduction in quantum efficiency going from matrix-isolated to adsorbed CF_3NO_2 gives some measure of the rate at which the surface participates in the relaxation of the excited state species. The photoproducts in this instance result from recombination of the nascent radicals, although this should also involve rotation of the fragments prior to recombination.

Gas phase studies of the collision products of $CF_3O + NO$[22] and $CF_3 + NO_2$[20] indicate that the $CF_2O + FNO$ products are the result of the decomposition of a four-center CF_3ONO intermediate, although this compound has not been definitively observed. The lack of significant CF_3NO_2 production in those experiments suggests that the rate constants governing the rearrangement of the intermediate into the nitro compound are negligible with respect to the primary product channel, although Garmanov and Vakhtin have noted some CF_3NO_2 production in their $CF_3 + NO_2$ study.[21] A recent paper by Oum and Hancock[40] postulates the existence of a possible five-center intermediate, responsible for the production of an unidentified (possibly FON) emission near 1880 cm^{-1}. They also observe weak emission near 1750 cm^{-1} which may be due to CF_3ONO, although they suggest other more probable assignments for this peak. Bevilacqua and co-workers[23] observe CF_3NO_2 or CF_3ONO (a peak at *m*/*e* 115) as a minor product of $CF_3 + NO_2$ collision. We may then envision the following kinetic scheme:

$$CF_3NO_2 \underset{k_r}{\overset{k_e}{\rightleftharpoons}} CF_3NO_2^* \underset{k_g}{\overset{k_f}{\rightleftharpoons}} CF_3\cdots NO_2 \xrightarrow{k_5} CF_3ONO \xrightarrow{k_6} CF_2O + FNO \quad (4)$$

where k_e is the zero-order rate constant for excitation, k_r, k_f, and k_6 are the first-order rate constants for relaxation, fragmentation, and intermediate fragmentation, respectively, and k_g and k_5 are the second-order rate constants for geminate recombination and intermediate formation, respectively. The $CF_3NO_2^*$ represents an excited-state parent species, and the $CF_3\cdots NO_2$ a radical pair trapped on-site. The apparent irreversibility beyond fragmentation allows the scheme to be simplified:

$$CF_3NO_2 \underset{k_r}{\overset{k_e}{\rightleftharpoons}} CF_3NO_2^* \underset{k_g}{\overset{k_f}{\rightleftharpoons}} CF_3\cdots NO_2 \xrightarrow{k_p} CF_2O + FNO \quad (5)$$

where k_p represents a second-order rate constant for product formation. This equation is similar in form to that derived in this group to describe the photochemistry of adsorbed CF_3NO,[10] where, once the second-order rate constants have been converted to their first-order equivalents, the quantum efficiency may be expressed as

$$\Phi \frac{k_p k_f}{k_p k_f + k_p k_r + k_r k_g} \quad (6)$$

The value of k_p may be obtained from the second-order constant obtained by Sugawara and co-workers[20] ($k = 2.5 \times 10^{-11}$ cm^3 $molecule^{-1}$ s^{-1}): taking the reaction volume to be that of one adsorption cell (2.24×10^{-23} cm^3 $molecule^{-1}$), yielding a k_p of 1.1×10^{12} s^{-1}. We may use the values of k_g from ref 10, $(0.3-3) \times 10^{12}$ s^{-1}, since the rate of recombination should not differ much for $CF_3 + NO$ or NO_2. Our best estimate of k_f comes from studies performed on CH_3NO_2,[41] where the fragmentation occurs within 5 ps, making k_f no larger than 2×10^{11} s^{-1}. The equation above may be solved for k_r:

$$k_r = \frac{k_p k_f}{k_p + k_g}\left(\frac{1 - \Phi}{\Phi}\right) \quad (7)$$

The values obtained for the rate constants may be found in Table 7.

TABLE 7: Derived Photophysical Parameters for Adsorbed CF_3NO_2

substrate	temp (K)	Φ	rate constants (s^{-1}) k_f[a]	k_g	k_p	k_r
NaBr	10	0.08	2×10^{11}	3.2×10^{12}	1.1×10^{12}	5.8×10^{11}
	70	0.20	2×10^{11}	4.5×10^{11}	1.1×10^{12}	5.8×10^{11}
KCl	80	0.09	2×10^{11}	4×10^{11}	1.1×10^{12}	1.5×10^{12}
	80	0.31	2×10^{11}	4×10^{11}	1.1×10^{12}	3.3×10^{11}
	80	0.12	2×10^{11}	4×10^{11}	1.1×10^{12}	1.1×10^{12}
KBr	10.5	0.31	2×10^{11}	3×10^{12}	1.1×10^{12}	1.2×10^{11}
	80	0.20	2×10^{11}	4×10^{11}	1.1×10^{12}	6.0×10^{11}
	80	0.24	2×10^{11}	4×10^{11}	1.1×10^{12}	4.7×10^{11}
	95	0.22	2×10^{11}	3.3×10^{11}	1.1×10^{12}	5.3×10^{11}
overlayer	11.2	0.29	2×10^{11}	2.8×10^{12}	1.1×10^{12}	1.4×10^{11}
	11.6	0.28	2×10^{11}	2.7×10^{12}	1.1×10^{12}	1.4×10^{11}
	50	0.35	2×10^{11}	6.3×10^{11}	1.1×10^{12}	2.3×10^{11}
	50	0.40	2×10^{11}	6.3×10^{11}	1.1×10^{12}	1.9×10^{11}
	80	0.32	2×10^{11}	4×10^{11}	1.1×10^{12}	3.1×10^{11}
	80	0.12	2×10^{11}	4×10^{11}	1.1×10^{12}	1.9×10^{11}

[a] Reference 41.

The relaxation rate constants obtained are consistent with those found for vibrational relaxation on these surfaces. The mechanism for quenching in this case requires some knowledge of the photochemical mechanism. Since little is known about the early stages of the process leading to the scission of the CN bond for this molecule, we will use CH_3NO_2 as a model. The surface phonons and/or excitons would be inefficient at relaxing the excited state molecule completely to the ground electronic state but could relax the excited state species to a nondissociating excited state. The long-wavelength band of CF_3NO_2, presumably an n,π^* transition, would leave the molecule near a low-lying triplet state emanating from the same configuration. In CH_3NO_2, the singlet−triplet separation is ~6300 cm^{-1}:[42] we would expect a similar separation for the perfluoro compound. The surface phonons would be able to accommodate this amount of vibrational energy, though there is no evidence that the n,π^* triplet state is any less dissociative than the n,π^* singlet state.

Another possibility is that the surface interferes with the terminal steps of the photochemical mechanism by destabilizing the intermediate, resulting in a smaller value of k_p, or by relaxing an excited state intermediate, also reducing k_p, but leading to a buildup of unreacted intermediate. We see little evidence of anything assignable to CF_3ONO (see below), making the latter supposition unlikely. The uncertainty in the derived relaxation constants make any estimate of the temperature dependence of relaxation unreliable. An exponential dependence of the relaxation constant would be expected for a vibrationally-based relaxation mechanism,[43] but the apparent independence of the quantum efficiency with respect to temperature indicates that there may also be a nonvibrational contribution to the relaxation process. A plot of the quantum efficiencies for the adsorbed and overlayer phases is shown in Figure 16. The enhanced quantum efficiency in the overlayer relative to that of the submonolayer coverage may be due to the alkali halide having a greater propensity to relax the excited state species or to an enhancement of k_p in the condensed phase.

The irradiations performed in these experiments, given the irradiation wavelength range, should result in the photolysis of

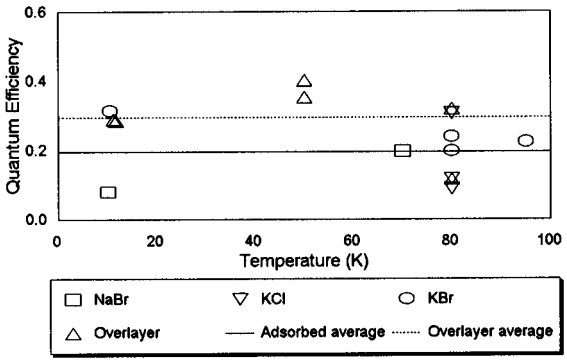

Figure 16. Temperature dependence of the quantum efficiencies of photolysis for submonolayer and multilayer CF_3NO_2 as a function of temperature. The lines represent the average values for the two phases.

photoproduct as well as parent species. Fortunately, the CF_2O does not undergo photolysis in this range and appears stoichiometrically with the loss of parent. The same cannot be said for the FNO. As a result, the FNO may be photolyzed, and its photoproducts likewise, until a nonphotolytic product is found, or the remnants desorb. Surface reaction seems to be the most likely scenario, given the abundance of defects on these surfaces and the affinity the nascent fluorine atoms would have for the apparently abundant negatively charged defects. On all but the NaCl films, weak peaks attributed to $(NO)_2$ are observed. Residual NO may desorb as a part of the FNO decomposition, but the design of the apparatus prevents ascertaining this. Oum and Hancock[40] indicate that the $CF_3 + NO_2$ reaction results in vibrationally excited FNO and CF_2O, with a minor channel leading to $CF_2O + F + NO$ (the branching ratio was estimated to be 1:0.015). The vibrational excitation in the FNO may be sufficient to allow desorption from the surface.

The one peak in the infrared that consistently appears as the result of photolysis on these films (and not attributed to CF_2O) occurs at $\sim$1184 cm^{-1}. This vibration could be a CF, NF, or NO stretch, depending on the compound. It is not present after the volatile adsorbates have been desorbed, indicating that it is not due to the formation of an NO_x surface ion. Despite the coincidence in frequency with the most prominent vibration of CF_3OONO_2 (observed in the N_2 matrix), we believe that CF_3OONO_2 is not being formed on these films. We do not observe any of the other prominent peaks for this compound and have no evidence of the presence of molecular oxygen on these films. In fact, experiments performed in this laboratory indicate that (a) oxygen coverage should be negligible on these films above 50 K and (b) irradiation of adsorbed CF_3NO_2 in the presence of coadsorbed O_2 at temperatures below 50 K demonstrated complete quenching of the photolysis of CF_3NO_2.[44] This peak may belong to the N−O stretch of the previously unobserved CF_3ONO molecule. An AM1 calculation[45] predicts the N═O stretching frequency for this molecule to be 0.8% above that of the parent compound, and as such, underneath the band of the nitro compound. The calculation also predicts an intense (213 km mol^{-1}) N−O stretching band within the frequencies bounded by the CF stretches of CF_3NO_2, which is the case for the 1184 cm^{-1} peak. However, the presence of only one peak in a very cluttered region of these spectra is certainly not enough evidence to ascertain the existence of this molecule in a stable form, especially in light of our inability to observe it in the argon matrix.

We do not observe any nitrate or nitrite as a result of photolysis. Other researchers have observed surface nitrate formation as a result of exposing these surfaces to NO_2, but indicate that coadsorbed water plays a role in the reaction.[46,47] Our experiments were designed to minimize the amount of water on these surfaces, which probably explains our lack of surface nitration.

The wealth of species found in the nitrogen matrices after irradiation gives evidence to the reactivity of the secondary photolysis products. The absence of concentration dependence in the photolysis efficiency is in agreement with the reported unimolecular mechanism. The production of CF_3OONO_2 as a result of irradiation of the most dilute nitrogen matrix was surprising, especially in light of quenching described above. The simplest imagined mechanism for production of this species would be an insertion of O_2 at the instant of fragmentation, but the amount of compound produced exceeds the amount expected from impurities (listed at <5 ppm) in the nitrogen. Similar concentrations of oxygen (<5 ppm) in the argon matrix would produce comparable amounts of this compound in those matrices, but none is observed. Additional oxygen resulting from FNO (or an atmospheric leak, even though we see little growth in condensed CO_2) decomposition seems to be finding its way to form N_2O, so there is some likelihood that atomic oxygen may also be present for reaction.

Conclusions

These experiments demonstrate some of the effects that a seemingly inert substrate may have on the photochemistry of an adsorbate. Adsorbed CF_3NO_2 is photolyzed with reduced efficiency and one of the initial photoproducts (FNO) apparently undergoes secondary photolysis. The relaxation rate constants were determined to be $(6 \pm 4) \times 10^{11}$ s^{-1} on the submonolayer coverage on the alkali halides and $(2 \pm 1) \times 10^{11}$ s^{-1} in the multilayer coverage. The alkali halide surfaces may well serve as a sink for the fluorine atoms produced in that secondary photolysis. These imply that the presence of airborne particulates will have some influence on the atmospheric stability and ultimate photochemical products of the fluorine-substituted nitromethanes that result from fluoromethyl−nitrogen dioxide collisions.[18]

The molecule appears to be adsorbed in an orientation that maximizes the interaction between the surface anion and the nitro group: most likely with the C−N bond parallel to the surface (along the {110} axis), with the trifluoromethyl group pointed toward the surface cation and the nitro group pointed toward a nearest neighbor cation. The desorption of the molecule was fit to first-order kinetics, and the derived rate constants were fit to an Arrhenius temperature dependence with an activation energy to desorption less than the molar heat of vaporization.

Acknowledgment. The authors acknowledge the support of the Faculty Research Committee of the University of Scranton. We also acknowledge the support of the Instrumentation and Laboratory Improvement program of the National Science Foundation (NSF-ILI USE-9250432) in the acquisition of the Fourier transform infrared spectrophotometer and vacuum equipment donations from Drs. Vince Barnett, Jeff Kiplinger, and Kevin Owens. The contributions made by Mary Roslonowski and Rance Prescott to this work are greatly appreciated. We also thank Professor Peter Cox for sharing some of his recent work with us.

References and Notes

(1) Barclay, V. J.; Hung, W.-H.; Keogh, W. J.; Kühnemuth, R.; Polanyi, J. C.; Zhang, G.; Zeiri, Y.; Jennison, D. R.; Li, Y. S. *J. Chem. Phys.* **1996**, *105*, 5005. Dixon-Warren, St. J.; Matyjaszczyk, M. S.; Polanyi, J. C.; Rieley, H.; Shapter, J. G. *J. Phys. Chem.* **1991**, *95*, 1333 and references contained in these.

(2) Tabares, F. L.; Marsh, E. P.; Bach, G. A.; Cowin, J. P. *J. Chem. Phys.* **1987**, *86*, 738.
(3) Barclay, V. J.; Jack, D. B.; Polanyi, J. C.; Zeiri, Y. *J. Phys. Chem.* **1993**, *97*, 12541 and references contained therein.
(4) Huang, Z.-H.; Guo, H. *J. Chem. Phys.* **1992**, *97*, 2110; **1993**, *98*, 7412. Fang, J. Y.; Guo, H. *J. Chem. Phys.* **1994**, *101*, 1231.
(5) Seideman, T. *J. Chem. Phys.* **1993**, *99*, 4766.
(6) Berg, O.; Ewing, G. E. *J. Phys. Chem.* **1991**, *95*, 2908.
(7) Dunn, S. K.; Ewing, G. E. *J. Phys. Chem.* **1993**, *97*, 7993; *Chem. Phys.* **1993**, *177*, 571.
(8) Willian, K.; Berg, O.; Ewing, G. E. *J. Chem. Soc., Faraday Trans.* **1996**, *92*, 4853.
(9) Richardson, H. H. *J. Phys. Chem.* **1992**, *96*, 5898.
(10) Giancarlo, L. C.; Haynie, B. C.; Miller, K. M.; Reynolds, J. M.; Rusnock, J. M.; Baumann, C. A. *J. Phys. Chem.* **1996**, *100*, 15539.
(11) Mason, J.; Dunderdale, J. *J. Chem. Soc.* **1956**, 759.
(12) Castelli, A.; Palm, A.; Alexander, Jr., C. *J. Chem. Phys.* **1966**, *44*, 1577.
(13) Karle, I. L.; Karle, J. *J. Chem. Phys.* **1962**, *36*, 1969.
(14) Tolles, W. M.; Handelman, E. T.; Gwinn, W. D. *J. Chem. Phys.* **1965**, *43*, 3019.
(15) Tolles, W. M. *J. Chem. Phys.* **1993**, *99*, 5718.
(16) Stephenson, E. H.; Macdonald, J. N. *J. Mol. Struct.* **1996**, *376*, 39.
(17) Cox, A. P.; Ellis, M. C.; Taleb-Bendiab, A.; Kuczkowski, R. L. *J. Mol. Struct.* **1996**, *376*, 51.
(18) Fazekas, G. B.; Takacs, G. A. *J. Photochem.* **1983**, *21*, 9.
(19) Rossi, M. J.; Barker, J. R.; Golden, D. M. *J. Chem. Phys.* **1989**, *71*, 3722.
(20) Sugawara, K.; Nakanaga, T.; Takeo, H.; Matsumura, C. *J. Phys. Chem.* **1989**, *93*, 1894.
(21) Garmanov, A. B.; Vakhtin, A. B. *Int. J. Chem. Kinet.* **1996**, *28*, 71.
(22) Chen, J.; Zhu, T.; Niki, H. *J. Phys. Chem.* **1992**, *96*, 6115.
(23) Bevilacqua, T. J.; Hanson, D. R.; Howard, C. J. *J. Phys. Chem.* **1993**, *97*, 3750.
(24) Li, Z.; Francisco, J. S. *Chem. Phys. Lett.* **1991**, *186*, 336.
(25) Wallington, T. J.; Schneider, W. F.; Szente, J. J.; Mariq, M. M.; Nielsen, O. J.; Sehested, J. *J. Phys. Chem.* **1995**, *99*, 984.
(26) Pitzer, K. S.; Brewer, L. (revision of Lewis, G. N.; Randall, M.) *Thermodynamics*, 2nd ed.; McGraw-Hill: New York, 1961; pp 674−680.
(27) Smart, R. St. C. *Trans. Faraday Soc.* **1971**, *67*, 1183.
(28) Woodward, A. J.; Jonathan, N. *J. Phys. Chem.* **1971**, *75*, 2930.
(29) Hohorst, F. A.; DesMarteau, D. D. *Inorg. Chem.* **1974**, *13*, 715.
(30) Taylor, W. D.; Allston, T. D.; Moscato, M. J.; Fazekas, G. B.; Kozlowski, R.; Takacs, G. A. *Int. J. Chem. Kinet.* **1980**, *12*, 231.
(31) Harmony, M. D.; Myers, R. J. *J. Chem. Phys.* **1962**, *37*, 636.
(32) Jacox, M. E.; Milligan, D. E. *J. Chem. Phys.* **1967**, *46*, 184.
(33) Comeford, J. J.; Mann, D. E.; Schoen, L. J.; Lide, D. R., Jr. *J. Chem. Phys.* **1963**, *38*, 461.
(34) Milligan, D. E.; Jacox, M. E. *J. Chem. Phys.* **1964**, *40*, 2461.
(35) Benedict, W. S.; Plyler, E. K. *Can. J. Phys.* **1957**, *35*, 1235; *J. Chem. Phys.* **1960**, *32*, 32.
(36) Moore, G. E.; Badger, R. M. *J. Am. Chem. Soc.* **1952**, *74*, 6076.
(37) Nielsen, A. H.; Burke, T. G.; Woltz, P. J. H.; Jones, E. A. *J. Chem. Phys.* **1952**, *20*, 596.
(38) Banus, J. *J. Chem. Soc.* **1953**, 3755.
(39) Jander, J.; Haszeldine, R. N. *J. Chem. Soc.* **1954**, 912.
(40) Oum, K. W.; Hancock, G. *J. Phys. Chem. A* **1997**, *101*, 2634.
(41) Schoen, P. E.; Marrone, M. J.; Schnur, J. M.; Goldberg, L. S. *Chem. Phys. Lett.* **1982**, *90*, 272.
(42) Flicker, W. M.; Mosher, O. A.; Kuppermann, A. *Chem. Phys. Lett.* **1979**, *60*, 518.
(43) Cassassa, M. P.; Heilweil, E. J.; Stephenson, J. C.; Cavanagh, R. R. *J. Chem. Phys.* **1986**, *84*, 2361.
(44) Roslonowski, M. Master's Thesis, University of Scranton, Scranton, PA, March 1994.
(45) HyperChem Release 4.5 for Silicon Graphics Workstations.
(46) Peters, S. J.; Ewing, G. E. *J. Phys. Chem.* **1996**, *100*, 14093.
(47) Langer, S.; Pemberton, R. S.; Finlayson-Pitts, B. J. *J. Phys. Chem. A* **1997**, *101*, 1277.